scientific reports

Check for updates

OPEN

MiR-322-5p is involved in regulating chondrocyte proliferation and differentiation in offspring's growth plate of maternal gestational diabetes

Fan Qian[1], Xianlong Chen[1], Simiao Wang[1], Yeyin Zhong[1], Min Liu[3], Guang Wang[1], Xuesong Yang[1,2]✉ & Xin Cheng[1]✉

Pregestational diabetes mellitus (PGDM) has an impact on fetal bone formation, but the underlying mechanism is still obscure. Although miRNAs have been extensively investigated throughout bone formation, their effects on fetal bone development caused by PGDM still need clarification. This study intends to examine the mechanism by which hyperglycemia impairs the bone formation of offspring via miR-322-5p (miR-322). In this study, miR-322 was selected by systemically screening utilizing bioinformatics and subsequent validation experiments. Using streptozotocin (STZ)-induced diabetic mice and ATDC5 cell lines, we found that miR-322 was abundantly expressed in the proliferative and hypertrophic zones of the growth plate, and its expression pattern was disturbed in the presence of hyperglycemia, suggesting that miR-322 is involved in the chondrocyte proliferation and differentiation in absence/presence of hyperglycemia. This observation was proved by manipulating miR-322 expression in ATDC5 cells by transfecting mimic and inhibitor of miR-322. Furthermore, Adamts5, Col12a1, and Cbx6 were identified as the potential target genes of miR-322, verified by the co-transfection of miR-322 inhibitor and the siRNAs, respectively. The evaluation criteria are the chondrocyte proliferation and differentiation and their relevant key gene expressions (proliferation: Sox9 and PthIh; differentiation: Runx2 and Col10a1) after manipulating the gene expressions in ATDC5 cells. This study revealed the regulative role miR-322 on chondrocyte proliferation and differentiation of growth plate by targeting Adamts5, Col12a1, and Cbx6 in hyperglycemia during pregnancy. This translational potential represents a promising avenue for advancing our understanding of bone-related complications in diabetic pregnancy and mitigating bone deficiencies in diabetic pregnant individuals, improving maternal and fetal outcomes.

Keywords Pregestational diabetes mellitus, miRNA-322-5p, Proliferation, Differentiation, Growth plate

There are roughly 223 million women with diabetes all over the world, based on the report in 2019, and the numbers are predicted to rise to 343 million by 2045. Of the women with diabetes, approximately 16.8% are attributed to gestational diabetes mellitus (GDM), while 13.6% are ascribed to pre-gestational diabetes mellitus (PGDM)[1]. Women with diabetes during pregnancy can affect their baby's development, such as the in-utero hyperglycemic environment, which can impair normal growth and mineralization of the fetal skeleton. It has been reported that the bone mineral density (BMD) of infants from insulin-dependent diabetic mothers is born with nearly 10% lower than the one from healthy pregnancy, and the ratio was inversely proportional to the glucose levels in diabetic pregnant women[2–4], and beta crosslaps (beta-CTX) were found to be elevated in the serum of diabetic mother, indicating the increased intrauterine bone resorption[4]. In addition to BMD reduction, diabetes

[1]Division of Histology and Embryology, International Joint Laboratory for Embryonic Development and Prenatal Medicine, Medical College, Jinan University, Guangzhou 510632, China. [2]Clinical Research Center, Clifford Hospital, Guangzhou 511495, China. [3]Key Laboratory of Functional and Clinical Translational Medicine, Fujian Province University, Xiamen Medical College, Fujian 350108, China. ✉email: yang_xuesong@126.com; tchengxin@jnu.edu.cn

during pregnancy also causes other fetal developmental abnormalities, including skeletal malformations and intrauterine growth retardation. The generalized retardation in skeletal maturation is well-documented in animal studies, such as the fewer ossification centers in the offspring of diabetic rats than in control ones[5]. If corrective action were not taken timely, diabetes during pregnancy would increase embryo resorption rates, fetal weight loss, and delayed skeletal development[6,7]. Clinical research uncovered a higher rate of congenital malformation in PGDM patients[8], in which there were 3.8% of major malformations and 0.7% of skeletal malformations[9]; 3 of the 12 anomalies in the offspring of maternal diabetes were embodied in skeleton[10]; tenfold increased risk of longitudinal limb defects, as well as sacral hypoplasia and abnormal spinal segmentation[11,12]. Our previous studies have shown that high glucose may negatively affect chicken embryos' skeletal development by influencing Wnt signaling[13]. Therefore, to carry out the prevention and cure work towards gestational diabetes-induced congenital malformation, it is imperative to clarify the underlying molecular mechanism of the effects of maternal diabetes on long bone formation in the stage of early embryonic development.

As we know, the development and growth of long bones is accomplished by the process known as endochondral ossification. Long bone formation begins with three-dimensional clumps of mesenchymal cells, which eventually differentiate into the chondrocytes, secreting a cartilage matrix. It is also called the cartilaginous model or anlage. Then, the centrally located chondrocytes convert from proliferation to differentiation while the chondrocyte size increases and changes into hypertrophic chondrocytes. Hypertrophic chondrocytes facilitate the mineralization of the surrounding matrix, tempt the invasion of blood vessels via secreting vascular endothelial growth factor (VEGF), and attract osteoclasts to break down the existing cartilage matrix. Meanwhile, osteoblasts derive from adjacent perichondral cells of hypertrophic chondrocytes and synthesize bone matrix to form a bone collar[14]. These regularly arranged chondrocytes (frequently organized into rows), i.e., growth plate, can be roughly divided into the following zones: resting zone (RZ), proliferative zone (PZ), hypertrophic zone (HZ), and calcified zone (CZ). The chondrocytes in the resting zone are round and small, serving as reserve cells; the chondrocytes in the proliferative zone are flattened; the chondrocytes in the hypertrophic zone remain columnar but become approximately 5–12 times larger. The terminally differentiated hypertrophic chondrocytes undergo apoptosis, vascular invasion, and replacement of mineralized bone. Throughout the process, the proliferative and hypertrophic zones of cartilage play essential biological functions in bone growth in length[14,15].

MicroRNAs (miRNAs) are small, non-protein coding RNAs that usually suppress gene expression by binding complementary sequences in the 3'-untranslated regions (3′-UTR) and then affecting either mRNA stability or protein translation[16]. Several studies indicated that miRNAs are involved in bone development[17]. For example, miRNA-26a is down-regulated in hypertrophic growth plate cartilage, and it can regulate chondrocyte hypertrophy by targeting CD200 and Col10a1 to inhibit ECM junction protein production, eventually implicating in maintaining extracellular matrix ECM homeostasis[18]; miRNA-374-5p, miRNA-379-5p, and miRNA-503-5p are abundantly expressed in the proliferative zone compared to the hypertrophic zone, and it is probably involved in contributing to establish concentration gradient of PTHrP, which in turn promotes proliferation and inhibits hypertrophic differentiation[19]. MiRNA-140 (miR140), which is the earliest discovered miRNA functioning in the development of cartilage, can inhibit myocyte enhancer factor 2 (CMEF2C), thereby regulating PTHrP/HDAC4 pathway and inhibiting hypertrophic differentiation[20]. The pathogenic phenotypes of the functionally acquired by miRNA mutation are derived from human miR140 mutation, which was similarly proved in miR140-deficient mice[21]. It is suggested that miRNAs are key modulators of bone development-related genes regulating endochondral bone formation.

In this study, we employed the streptozotocin (STZ)-injected diabetic mouse model and ATDC5 (chondrocyte cell line) cells to systemically investigate the effect mechanism of miR-322 on fetal bone development in the context of having diabetes during pregnancy.

Materials and methods

Microarray data and identification of differentially expressed genes

Gene expression omnibus (GEO) (http://www.ncbi.nlm.nih.gov/geo)[22] is a public functional genomics data repository providing high-throughput gene expression data. In this study, the GSE98036 and GSE7685 datasets were downloaded from GEO. The growth plate from mouse limb bones can be partitioned into three distinct zones; in this study, the proliferative and hypertrophic zones were chosen for further analysis. Different miRNA (differentially expressed miRNA, DEM) and mRNA (differentially expressed mRNA, DEG) in the PZ and HZ of the growth plate were processed using R software. The downloaded raw data were first processed with affy R package, and then limma was used for the analysis of differential gene expression to obtain DEM and DEG. The conditions for differential genetic discrimination were set to $|\log2FC| \geq 1.5$ and $P < 0.05$. Clustering analysis was performed and DEM/DEG heat maps were drawn using the heatmap package.

Enrichment analyses and miRNA-mRNA network identification

All target genes were submitted to the DAVID database (https://david.ncifcrf.gov) for gene ontology (GO)[23] and Kyoto encyclopedia of genes and genomes (KEGG)[24] enrichment analysis. The threshold was set at $P < 0.05$. Using miRDB (http://www.mirdb.org/), TargetScan (http://www.targetscan.org/vert_72/), Starbase (https://starbase.sysu.edu.cn/starbase2/) and Tarbase (multiMiR package) to predict target genes of DEM. The predicted genes from these four databases were pooled into a single database, and the intersection of the DEG with this database was considered as significantly differentially expressed target genes. Cytoscape was used to identify the miRNA-mRNA network.

Search strategy and study selection

We conducted a comprehensive search for the correlations between diabetes during pregnancy and fetal bone development, using search phase "(pregnancy OR gestational) and (diabetes OR diabetes mellitus OR diabetic) and (baby OR infant OR fetal OR fetus OR embryo OR embryonic OR offspring OR newborn OR birth OR outcome) and (bone OR limb)" to conduct executive research. The search phases "(miR OR microRNA OR miRNA) and (growth plate OR epiphyseal cartilages OR epiphyseal plate)" were used to search for the role of miRNA in growth plate during fetal bone development. After screening the titles and abstracts, we carefully viewed full text to determine whether the articles meet inclusion/exclusion criteria. Only the peer-reviewed studies with specific data were included. The exclusion criteria were (1) non-empirical studies, including reviews, case-reports, conference abstracts, letters; (2) the duplicated studies; (3) the irrelevant studies. Two authors independently checked the eligibility of all the identified studies. In case of disagreement, the two researchers would reach a consensus decision through a critical discussion.

Mouse model

The C57BL/6 mice utilized in this investigation were sourced from the Institute of Laboratory Animal Science at Jinan University (Guangzhou, China). Female mice at eight weeks of age were employed to induce diabetes mellitus by administering 2% streptozotocin (STZ) solution, dissolved in 0.01 M citrate buffer at a pH of 4.5, at a dosage of 75 mg/kg body weight for three consecutive days. Blood glucose levels were assessed seven days following the STZ injection using the Roche Accu-Chek Aviva Blood Glucose System (Roche). Diabetes mellitus was defined as a fasting blood glucose level exceeding 288 mg/dL (16 mM) following established criteria. Control mice were maintained at normal blood glucose levels (4–8 mM) before and during pregnancy. Throughout pregnancy, blood glucose levels were monitored at six-day intervals. Pregnant mice were euthanized by sodium pentobarbital at E18.5 and the embryos were removed by laparotomy. All procedures involving animal treatment in this study adhered to the protocols of the Jinan University Animal Experimental Ethics Committee. All processes involving animal treatments in this study were in accordance with the procedures of Ethical Committee for Animal Experimentation, Jinan University (IACUC-20181126-02). All experimental procedures were conducted in conformity with the institutional guidelines issued by the ARRIVE guidelines.

Cell culture and transfection

Chondrogenic cell line ATDC5 (ATCC, Manassas, VA) cells were cultured in Dulbecco's Modified Eagle Medium (DMEM, Gibco) supplemented with 10% fetal bovine serum (FBS, Gibco, Gaithersburg, MD). To induce chondrogenic differentiation, the culture medium was supplemented with insulin–transferrin–sodium selenite media supplement (ITS, Sigma) for 7 days. 50 mM D-glucose (Sigma, MO, USA) were used as high glucose, 25 mM as normal glucose. Additionally, 50 mM mannitol was used as an osmotic control. The miR-322 mimic, miR-322 inhibitor, si-Adamts5, si-Col10a1, and si-Cbx6 molecules were obtained from RiboBio (Guangzhou, China). Non-specific microRNA mimic, inhibitor, and siRNA molecules were used as negative controls (NC mimic, NC inhibitor, and si-NC). The cells were transfected with 100 nM siRNA, 50 nM mimic, or 100 nM inhibitor using Lipofectamine 3000 (ThermoFisher, USA) for 6 h. After 24 h, cells were harvested for qRT-PCR assay.

Hematoxylin and eosin (H&E), alcian blue and alizarin red staining

The femurs of the mouse embryos were collected from control and STZ-treated mice. Bone histological analyses on H&E staining were performed with longitudinal sections using standard protocols.

The alcian blue and alizarin red dyes for the whole embryo were as previously described[25]. The mouse embryos were carefully isolated from surrounding tissues, and then they were subjected to fixation in 95% ethanol for a period of 2 days. Subsequently, the embryos were further fixed in acetone for an additional day. To highlight the cartilage, the embryos were stained with alcian blue, and for bone visualization, they were counterstained with alizarin red (Solarbio, Beijing, China). The specimens were meticulously dissected, and images were captured using a stereomicroscope.(MVX10, Olympus, Tokyo, Japan). The lengths of each bones were quantitatively analyzed using Image Pro-Plus 5.0 software (IPP, Media Cybernetics)[26].

Immunofluorescence staining

The tissue slides or cells were fixed with 4% PFA and washed by PBS. Monoclonal primary antibodies against were performed at 4 °C overnight: PCNA (1:200, Abcam, ab92552, USA), Runx2 (1:200, Abcam, ab192256, USA), Ki67 (1:200, Abcam, ab15580, UK), Col10a1 (1:200, Abcam, ab260040, USA)**.** The secondary antibody were Alexa Fluor 555 anti-rabbit IgG (1:1000, Invitrogen, CA, USA) or Alexa Fluor 488 anti-rabbit IgG (1:1000, Invitrogen, CA, USA), usually counter-staining with 4'-6-diamidino-2-phenylindole (DAPI, 5 μg/mL, Life Tech, USA) to reveal the nuclei. The slides were photographed by an Olympus IX51 microscope (Olympus, Tokyo, Japan). Details are provided in Supplementary Table S1. The immunofluorescent intensity was quantitative measured as previously describe[27–30]. The results were analyzed using image J software.

Fluorescence in situ hybridization (FISH)

RNA FISH SA-Biotin kit (GenePharma, China) was used for RNA fluorescence in situ hybridization on the longitudinal slides of mouse growth plate as previously described[31,32].

RNA isolation and quantitative PCR (q-PCR)

Total RNA was extracted by Trizol (Invitrogen, Waltham, MA, USA) from the harvested mouse femurs (Fig. S3) and ATDC5 cells. MiRNA-322-5p was using specific primer (20 μM): GTCGTATCCAGTGCAGGGTCCGAG

GTATTCGCACTGGATACGACTCCAAA. The other primers' sequences are provided in Supplementary Table S2. The PCR reactions were performed in a Bio-Rad S1000TM Thermal cycler (Bio-Rad, Hercules, CA, USA) as described previously[33,34]. The expression of these genes was normalized to β-actin and compared by ΔΔCt. The Plots was performed using GraphPad Prism 8 software.

Data analysis

The statistical analysis of the experimental data was performed using SPSS Statistics 26.0 software. Graphical representations were generated using GraphPad Prism 8 software. Each experiment was repeated three times, and the data are presented as mean ± SD. Statistical comparisons between groups were conducted using *t* text,, one-way ANOVA, and other appropriate statistical methods. $P < 0.05$ was considered statistically significant, denoted by "*". The symbols "**" and "***" were used to indicate statistical significance when the P-value was less than 0.01 and 0.001, respectively.

Results

The pathology of bone development in infant of diabetic pregnancy.

To explore the relevance between diabetes mellitus during pregnancy and fetal bone development, totally, 1812 relevant articles were consulted in the Pubmed database. Based on the abstracts, 133 articles were selected after excluding animal study and review articles, of which 27 satisfied the inclusion criteria (Fig. S1A). The phenotypes of bone development included bone mineral density, bone length, sacral insufficiency and malformation. Of the 27 articles, there were 6 low bone mineral density in fetus, 17 congenital short bone, 5 sacral insufficiency fractures, and 9 limb malformations (Fig. S1B). All of these implied that diabetes during pregnancy had a significant impact on fetal bone development.

Additionally, alcian blue/alizarin red staining showed that the lengths of the humerus, radius, ulna, femur, fibula, and tibia of E18.5 pre-gestational diabetes mellitus (PGDM) mouse embryos were significantly shorter than those of control embryos (Fig. 1A–D). H&E staining on longitudinal sections of the femur showed that the proportion of the growth plate relative to the entire bone length increased in PGDM mouse embryos (Fig. 1E,G); there was no significant difference in the proportion of RZ and PZ to the whole length of the growth plate despite a substantial increase in the relative length of HZ to the whole growth plate (Fig. 1F,H). It is suggested that diabetic pregnancy led to the pathological development of embryonic long bones, which was manifested as shortened bone length, increased proportion of growth plates, and prolonged hypertrophic zone, which reminds us of the necessity to explore the underlying mechanism.

miRNA plays an essential regulatory role in long bone development.

One hundred twenty-three relevant articles were found in the Pubmed database for further analyzing the relationship between miRNA and long bone developmeThirty-seven. 37 articles were finally selected, and 9 of them met the inclusion criteria (Fig. S2A). According to the miRNAs-involved enrichment location and their function, we found that miRNAs could affect chondrocyte proliferation or differentiation in the proliferative or hypertrophic region within the 9 articles (Fig. S2B). This implies that miRNAs indeed play an regulatory role in long bone development through targeting growth plate.

The effects of miRNAs on the proliferative and hypertrophic regions of the growth plate were screened out using the GSE98036 dataset, and 12 differentially expressed miRNAs (DEMs) were obtained, of which 10 were up-regulated and 2 were down-regulated (Fig. 2A). GO and KEGG analyses of DEMs were performed in miEAA[35], and showed their biological functions in mouse growth plate (Fig. 2B,C). Furthermore, a total of 1112 differentially expressed genes (DEGs) were obtained in the GSE7685 dataset, of which 400 were up-regulated and 712 were down-regulated (Fig. 2D). Since miRNA usually correspond with multiple genes, we used several databases including miRDB, TargetScan, Starbase and Tarbase to predict the DEMs' target genes. The VENN map showed the 37 overlapping target genes between DEMs' target genes and DEGs, which were considered as more important genes in total differently expressed genes on PZ and HZ (Fig. 2E). Then, we found that only miR-322-5p, miR-22-3p and miR-181a-5p were correspond with the 37 overlapping target genes. The miRNA-mRNA regulatory network constructed by Cytoscape 3.9.1 was taken to show the relationship of the 37 overlapping target genes in Fig. 2E and the miRNAs (miR-322-5p, miR-22-3p and miR-181a-5p) (Fig. 2F). To explore the role of overlapping target genes in biological functions, GO and KEGG pathway analysis was performed. The results of the GO enrichment analysis of the three modules indicated the biological process, cellular components, and molecular function, respectively (Fig. 2G). The results of KEGG enrichment analysis demonstrated the miRNAs in cancer and MAPK signaling pathway in regulating actin cytoskeleton (Fig. 2H). Taken together, the miRNA-mRNA regulatory networks might really involve in regulating the biological functions of growth plate chondrocytes.

miR-322 regulates the proliferation and differentiation of long bone chondrocytes in PGDM embryos.

The heatmap plot showed that miR-322 was the most significantly up-regulated miRNA in the hypertrophic region, so we focused on the effect of miR-322 on chondrocyte proliferation and differentiation in growth plate below (Fig. 3A). The expression pattern of miR-322 in growth plates of mouse femur were examined using q-PCR and fluorescence in situ hybridization (FISH). The q-PCR result showed the higher miR-322 expression in HZ than PZ in control, but the opposite trend was found in PGDM group (Fig. 3E), which was confirmed by FISH in femur growth plate (Fig. 3B–D). To further investigate the abnormal expression of miR-322 in the proliferative and hypertrophic regions of the growth plate of PGDM mice, we cultured ATDC5 in the context of a high glucose for 24 h and then detected the expression of miR-322. The result showed that after 24 h of culture, the expression level of miR-322 increased compared with the normal group, and there was no significant difference

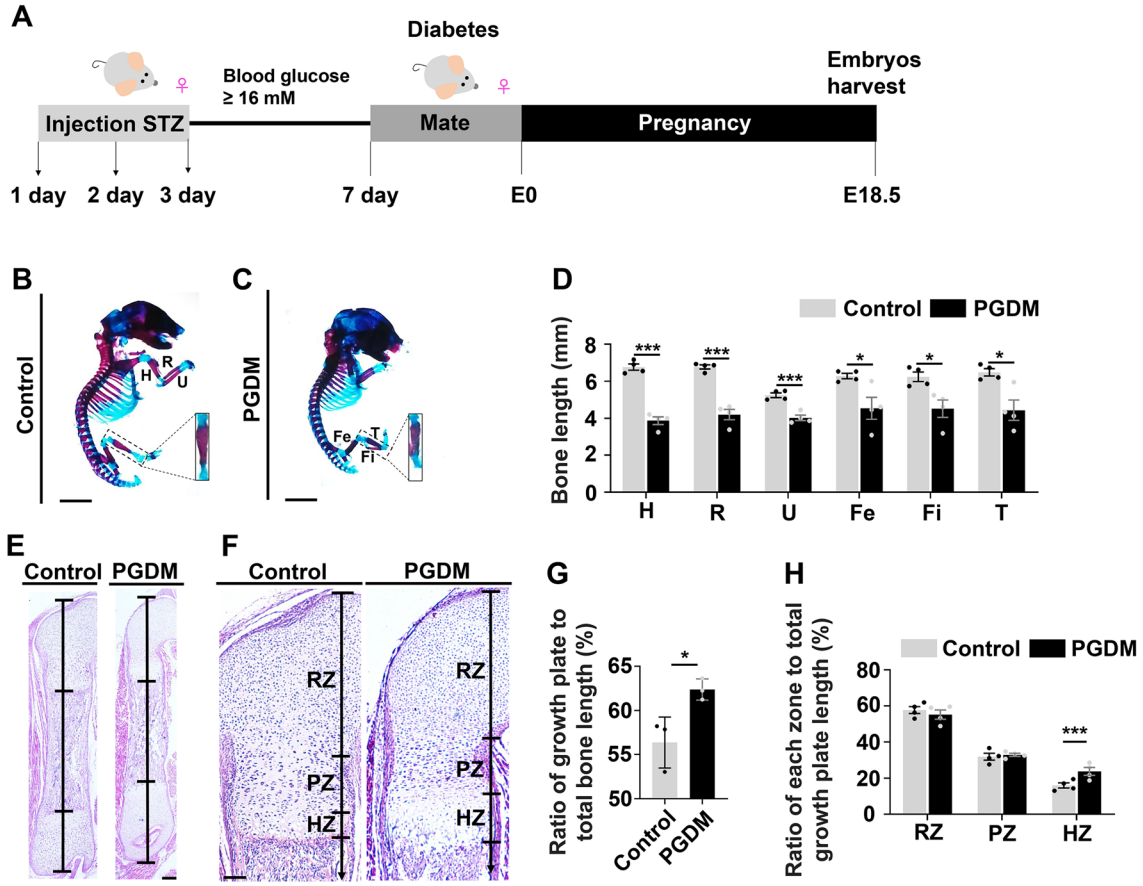

Figure 1. Assessing the long bone development in the offspring of pregnant mice with diabetes. (**A**) Schematic illustration of the establishment of pregestational diabetes mellitus (PGDM) mouse model and the harvest point-in-time of offspring. (**B**,**C**) Representative alcian blue/alizarin red stained images of E18.5 mouse embryos from control (**B**) and PGDM (**C**) groups. (**D**) Bar graph showing the comparison of average length of the humerus (H), radius (R), ulna (U), femur (Fe), fibula (Fi) and tibia (T) of E18.5 mouse embryos from control (n = 4) and PGDM (n = 4) groups. (**E**,**F**) Representative H&E stained images of the full-length femur (**E**) or femoral growth plates (**F**) of E18.5 mouse embryos from control and PGDM groups. (**G**,**H**) Bar charts showing the ratio of the growth plate to the entire femoral length (**G**) or the ratio of the RZ, PZ and HZ lengths to the growth plate length (**H**) for the control (n = 3–4) and PGDM (n = 3–4) groups. *RZ* resting zone, *PZ* proliferative zone, *HZ* hypertrophic zone. Scale bars for (**B**,**C**) = 5 mm; (**E**,**F**) = 200 mm. Each bar represents mean ± S.D.; Student's t-test: $^{*}P < 0.05$, $^{**}P < 0.01$, $^{***}P < 0.001$.

between the osmotic pressure control and the control group (Fig. 3E). In contrast, the expression of miR-322 was down-regulated after 7 days of incubation in the context of high glucose (Fig. 3F), which was consistent with the in vivo results. It was hypothesized that miR-322 was associated with the proliferation and differentiation of chondrocytes.

Then the in vitro experiments of ATDC5 cells were employed to study chondrocyte proliferation and relevant key gene expression when up-regulating or down-regulating miR-322 through the transfection of miR-322 mimic or inhibitor in ATDC5 cells after cultured in the context of neither normal or high glucose environment(Fig. 4A,B, Fig. S4A–C). Q-PCR data manifested that high glucose inhibited the expressions of Sox9 and PthIh; up-regulation of miR-322 (miR-322 mimic) significantly increased both gene expressions; down-regulation of miR-322 (miR-322 inhibitor) significantly regressed the both gene expressions (Fig. 4C,D). Likewise, we found the same variation trend in the Ki67-fluorescently labeled chondrocyte proliferation in the absence/presence of high glucose (Fig. 4E,E1), implying the stimulative effect of miR-322 on chondrocyte proliferation in the growth plate, which became more pronounced in the presence of high glucose.

Using the same strategy, we investigated the effect of miR-322 on chondrocyte differentiation following the 7 days differentiation-culture medium incubation after transfection in the context of neither normal or high glucose environment (Figs. 3G, 5A, Fig. S4D,E). Quantitative PCR showed the inhibitive expression of Runx2 and Col10a1 in miR-322 mimic group, but significant increase in miR-322 inhibitor groups (Fig. 5B,C). Alcian blue staining showed that entire chondrocyte spheroids with miR-322 inhibitor reversed the decrease of miR-322-induced chondrocyte differentiation (Fig. 5D). Furthermore, immunofluorescent staining of Runx2 (Fig. 5E) and Col10a1 (Fig. 5F) in ATDC5 cells showed that high glucose inhibited both gene expressions; blocking miR-322 with miR-322 inhibitor transfection re-up-regulated the expressions of Runx2 and Col10a1, which have been

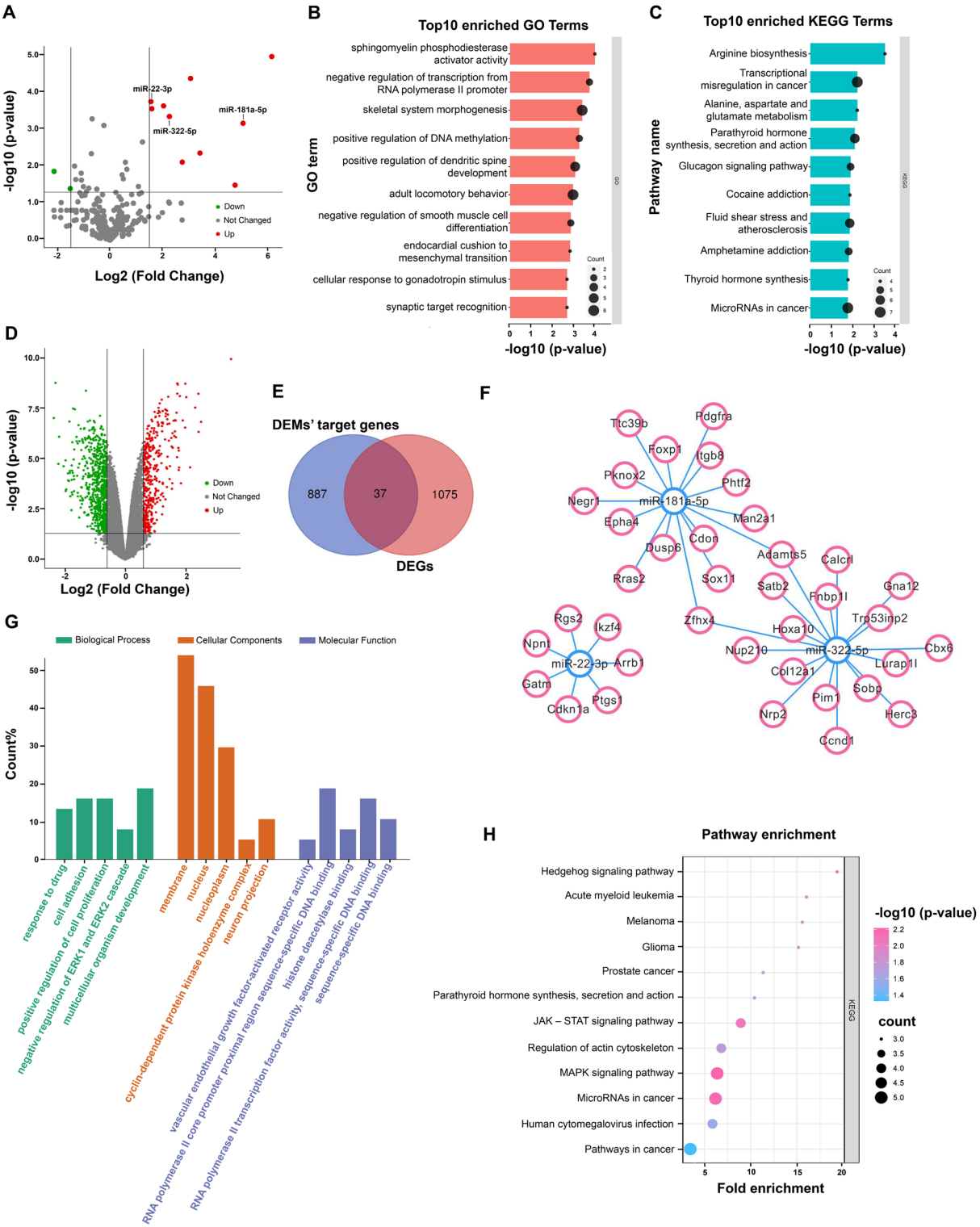

suppressed by over-expressing miR-322 with miR-322 mimic transfection (Fig. 5E1,F1). These data indicated that miR-322 might inhibit chondrocyte differentiation, especially in the presence of high glucose.

The regulatory effect of miR-322 on chondrocyte proliferation and differentiation in the growth plate was achieved by targeting Adamts5, Col12a1, and Cbx6

To uncover the mechanism for miR-322 regulatory effect, we employed those mentioned intersecting regulatory networks of miRNA322-mRNA to screen potential target genes (Fig. 6A,B). The results indicate that Adamts5, Col12a1, and Cbx6 mRNA could be the potential target genes since they were decreased upon miR-322 mimic transfection and increased by miR-322 inhibitor transfection (Fig. 6C,D).

◂**Figure 2.** Bioinformatic analysis of miRNA-mRNA regulatory networks in growth plate. (**A**) The volcano plot using |log2FC|≥1.5 and $P<0.05$ as cut off values for DEM (differentially expressed miRNA) in the proliferative and hypertrophic regions of the growth plate using the GSE98036 dataset. Note: red dots represent up-regulated DEM (n=10), green dots represent down-regulated DEM (n=2), and gray dots represent non-DEM. (**B**,**C**) The top 10 results of GO (**B**) and KEGG (**C**) analysis enriched by DEM in miEAA (microRNA enrichment analysis and annotation). Note: the bars were sorted by *p*-value; the size of the bubbles indicates the degree of enrichment, with larger bubbles reflecting a higher gene ratio. (**D**) The volcano plot using |log2FC|≥1.5 and $P<0.05$ as cut off values for DEG (differentially expressed gene) in the proliferative and hypertrophic regions of the growth plate using the GSE7685 dataset. Note: red dots represent up-regulated DEG (n=400), green dots represent down-regulated DEG (n=712), and gray dots represent non-DEG. (**E**) The overlapping genes between DEGs and DEM's target genes which prodected from miRDB, TargetScan, Starbase and Tarbase . Note: blue circle represent DEM's target genes, and red circle represents DEGs. (**F**) The miRNA-mRNA regulatory network with 40 nodes and 39 interactions (**F**). Note: a red circle represents mRNA, and a blue circle represents miRNA. (**G**,**H**) GO (**G**) and KEGG (**H**) analysis using DAVID database for overlapping target genes. Note: the top 5 GO functional annotation in three modules were screened as different colors; a bobble plot depicting enriched pathways; red indicates a high *p* value and blue indicates a low *p* value; the size of the bubbles indicates the degree of enrichment, with larger bubbles indicating a higher gene ratio.

To further confirm that miR-322 regulates proliferation and differentiation by targeting Adamts5, Col12a1, and Cbx6, we manipulated the Adamts5, Col12a1, and Cbx6 mRNA levels by transfecting siRNAs in ATDC5 cells (Fig. 7A,F,N). The Quantitative PCR results showed that inhibiting Col12a1 (Fig. 7C,D) and Cbx6 (Fig. 7H,I) expressions by transfecting their inhibitors could significantly reverse the increase of Sox9 and PthIh expressions induced by transfecting Si-Col12a1 or Si-Cbx6 only, but no similar trend was found when Admts5 was inhibited by its inhibitor transfection (Fig. 7M,N). Immunofluorescent staining of PCNA in ATDC5 cells, which were similarly manipulated by transfections of their corresponding siRNAs, also manifested that inhibiting Col12a1 or Cbx6 expressions by transfecting their inhibitors could significantly reverse the increase of chondrocyte proliferation induced by transfecting Si-Col12a1 or Si-Cbx6 only (Fig. 7E-E1,J-J1,O-O1).

The same strategy was used to assess the effects of Adamts5, Col12a1, and Cbx6 as the target genes of miR-322 in chondrocyte differentiation (Fig. 8). Quantitative PCR results showed the increase of Runx2 expression after inhibiting Adamts5, Col12a1, or Cbx6 expressions by transfecting their inhibitors (Fig. 8A,F,K); as well as the increase of Col10a1 expression after inhibiting Adamts5 or Col12a1 expressions (Fig. 8B,G,L). And the immunofluorescent staining of Runx2 (Fig. 8C-C1,H-H1,M-M1) and Col10a1 (Fig. 8E-E1,J-J1,O-O1) was implemented in ATDC5 cells, in which the expression levels of Adamts5, Col12a1, and Cbx6 were manipulated by transfections of their corresponding siRNAs. A similar trend was observed in alcian blue staining (Fig. 8D,I,N).

Discussion

The STZ-induced diabetic model has been widely used since it can reliably offer an experimental platform to research mammalian diabetes[36]. In this study, the diabetic mouse model demonstrated the endochondral bone growth restriction, and we assumed that the pathological mechanism was involved in the accumulation of proliferative chondrocytes in the proliferative zone, i.e., disturbance of coordinated proliferation and differentiation of chondrocytes, which gives the assurance of incessant elongation of the epiphyseal growth plate. Based on these experimental results, we presume that MiRNA-322-5p (miR-322) plays an important role in the pathology of diabetic complications. The miR-322 is a new-found factor in regulating the functions of osteoblasts and osteoclasts during osteogenesis. For instance, it has been described that miR-322 stabilizes MEK1 expression by inhibiting RAF/MEK/ERK pathway in cartilage cells[37] and modulating Osterix mRNA stability by targeting Tob2[38]. Meanwhile, miR-322 has also been found to be down-regulated in the embryos of nondiabetic and diabetic dams, indicating that maternal diabetes and hyperglycemia had a negative regulative effect on miR-322, which represses the translation of TRAF3 by interacting with 3'-UTR of TRAF3 in neural progenitor cells[39].

However, no studies have been conducted to establish potential miRNA-mRNA regulatory networks during cartilage development to provide novel prospects for understanding abnormal development of long bone. In this study, a miRNA-mRNA regulatory network potentially involved in the process from PZ to HZ was first constructed using GEO datasets. The 3 miRNAs and 39 mRNAs were consequently identified by miRDB, TargetScan, Starbase, and Tarbase (Figs. 1, 2). Of all these nodes, miR-322 was significantly up-expressed in the hypertrophic zone of the growth plate (Fig. 3).

miR-322 plays a crucial role in cartilage formation. Previous studies have indicated that miR-322, which is up-regulated by Sox9, directly targets Smad7, leading to increased cartilage differentiation and reduced hypertrophic differentiation, decreased early apoptosis rate of MSCs, and assisting BMP2 in promoting cartilage formation[40]. Additionally, experimental research conducted by Bluhm et al. demonstrated that miR-322 inhibits RAF/MEK/ERK pathway activation in cartilage cells[37]. Moreover, the expression and function of miR-322 may vary depending on the location. miR-322 and miR-503 are highly expressed in the prehypertrophic/hypertrophic zone of the growth plate and articular cartilage. They could stimulate RANKL or reduce OPG expression, inducing osteoclast formation and bone remodeling at the cartilage-bone junction[41]. In mice with genetic ablation of the cartilage-specific Mirc24 cluster encoding miR-322 (Col2a1-Cre-Mirc24tm1M mice), key transcription factors involved in ECM production, such as SOX9 and its co-factor SOX6, have been found significantly down-regulated[42]. Additionally, the level of miR-322 was decreased in the damaged cartilage of mice with destabilized meniscus-induced osteoarthritis[43], suggesting a potential involvement of miR-322 in cartilage homeostasis and degeneration. Interestingly, offspring of low-birth-weight non-catch-up growth (LBW-NCG) rats exhibited high expression of miR-322 and low expression of GHR and IGF-1 in the liver. Overexpression of miR-322 suppressed

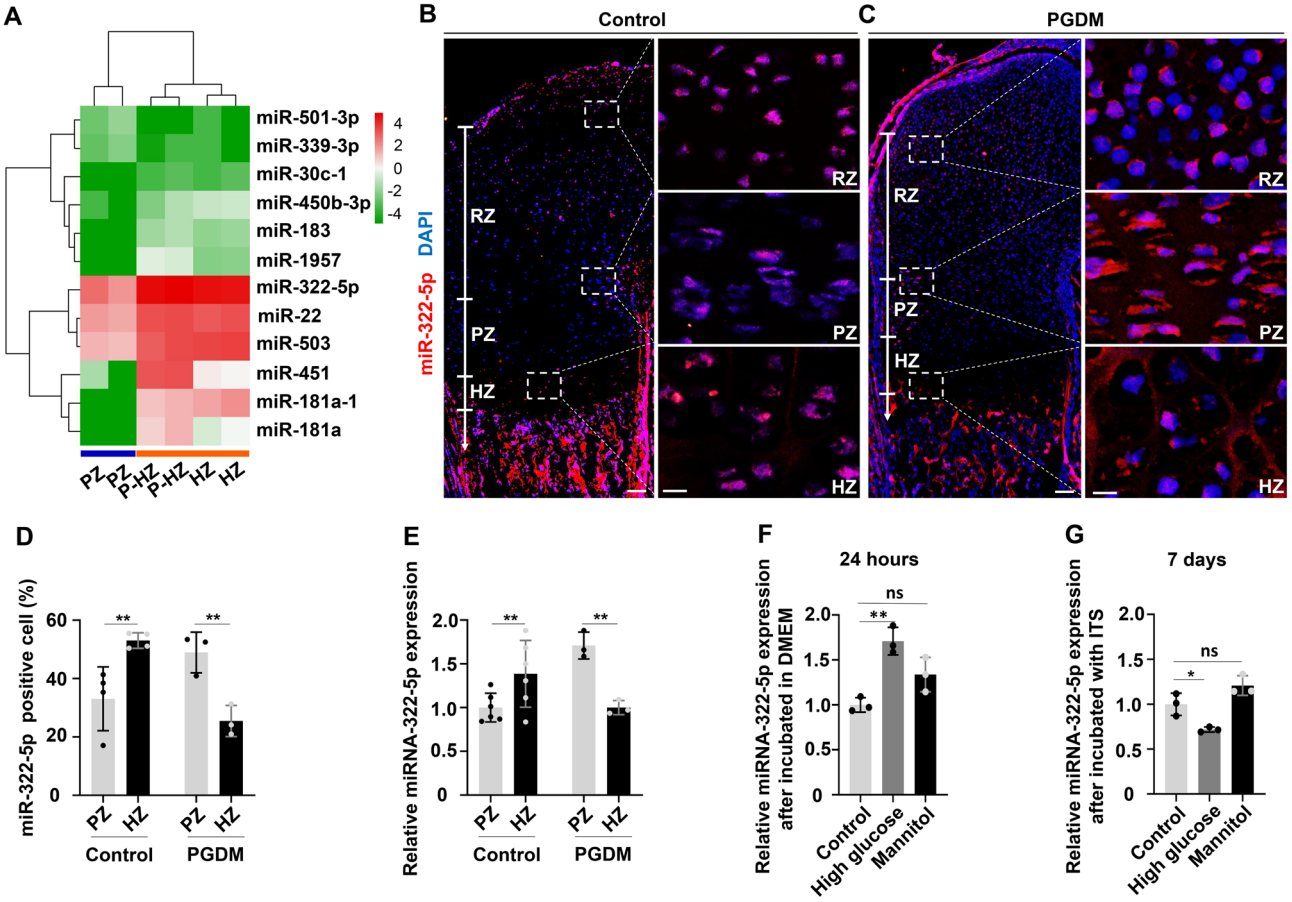

Figure 3. miR-322 is chosen and its expression on growth plate of control and PGDM mouse femur. (**A**) A heat map depicting a variety of 12 DEM expression in PZ and HZ (combined with P-HZ) of growth plate (Note: P-HZ represents Pre-hypertrophic zone). (**B**,**C**) Representative images of miR-322 fluorescence in situ hybridization (FISH) in RZ, PZ and HZ from control (**B**) and PGDM (**C**) groups. All slides were counterstained with DAPI. (**D**) Bar charts showing the comparisons of relative fluorescence intensities of miR-322 in PZ and HZ from control (n = 4) and PGDM (n = 3) groups. Each bar represents mean ± S.D.; Student's t-test.: $^{*}P < 0.05$, $^{**}P < 0.01$, $^{***}P < 0.001$. (**E**) q-PCR data showing the expression of miR-322 in PZ and HZ from control and PGDM mouse embryos. Student's t-test, n = 5 for control and n = 3 PGDM groups, respectively. (**F**,**G**) The q-PCR data showing the expression of miR-322 in ATDC5 cells in the incubation time of 24 h (for cell proliferation) (**F**) or 7 days (in presence of ITS—for cell differentiation) (**G**) in control, mannitol (as osmotic control) and high glucose groups (n = 3, respectively). Scale bars 200 μm in the left of (**B**,**C**), 10 μm in the right of (**B**,**C**). Each bar represents mean ± S.D.; ANOVA: $^{*}P < 0.05$, $^{**}P < 0.01$, $^{***}P < 0.001$.

the expression of the growth hormone receptor (GHR), and inadequate calorie intake during pregnancy led to catch-up growth failure. The authors also observed reduced expression of the GH receptor in the tibial cartilage of non-catch-up low birth weight rats, suggesting a potential increase in miR-322 expression in the cartilage of low birth weight rats. However, the specific mechanism is unknown[44].

Here, we found that the expression of miR-322 was specifically suppressed in the PGDM-enlarged hypertrophic zone of the mouse growth plate and enhanced in the proliferative zone at the same time (Fig. 3). Based on these observations, we speculate that the miR-322 role is probably complicated in the hyperglycemia-induced pathological process of bone development. This is to say that the altered expression of miR-322 expression in the context of hyperglycemia might directly cause chondrocyte proliferation and differentiation by targeting relevant genes.

So, we next intended to explore if miR-322 regulated chondrocyte proliferation and differentiation at the growth plate in the context of hyperglycemia. In order to verify this speculation, we determined the expressions of Sox9 and PthIh, the chondrocyte proliferation-related genes, in the ATDC5 cells that miR-322 level was manipulated through the transfections of miR-322 negative control (NC), its mimic or inhibitor in absence/presence of high glucose (Fig. 4). The following results were shown: (1) high glucose inhibited the expressions of Sox9 and PthIh; (2) inhibiting miR-322 by transfection of its inhibitor could significantly reverse miR-322-induced the increased of Sox9 and PthIh expressions; (3) likewise, the increased Ki67-labeled chondrocyte proliferation caused by miR-322 mimic transfection was significantly regressed again by miR-322 inhibitor transfection in presence of high glucose (Fig. 4). Using the same strategy, we uncovered the miR-322 inhibitor transfection successfully reversed the expressions of chondrocyte differentiation-related genes, Runx2 and Col10a1, as well as

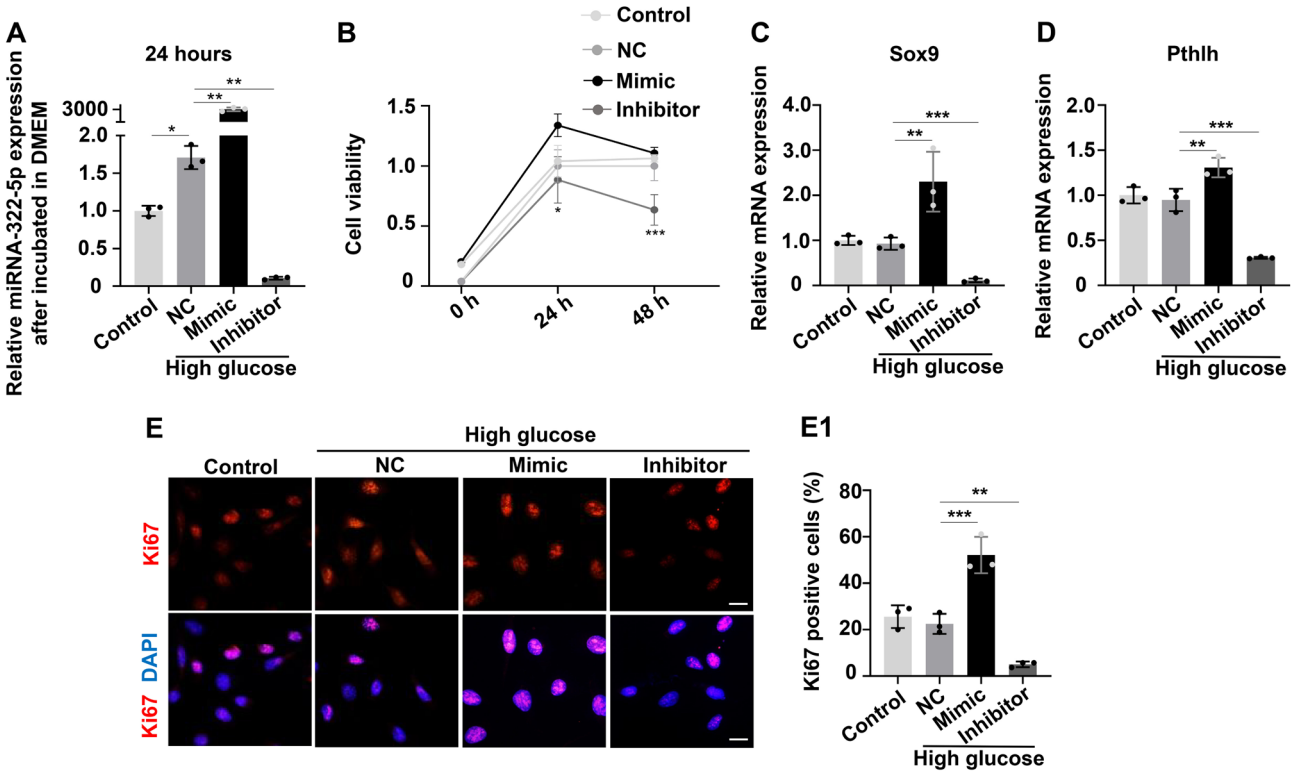

Figure 4. Determining the proliferation of chondrocytes in ATDC5 cells in presence of high glucose environment after manipulating miR-322 level. (**A**) The qRT-PCR data showing the expression level of miR-322 in ATDC5 cells in different groups (Note: NC represents negative control of miR-322 mimic and inhibitor) following 24-h transfection. (**B**) The cell viability in different groups was detected using CCK8 after 24- and 48-h incubation following transfection. (**C**,**D**) q-PCR data showing the expression of sox9 (**C**) and pthlh (**D**) in ATDC5 cells transfected with miR-322 mimics or inhibitor. (**E**,**E1**) Representative Ki67 staining following the transfection of miR-322 mimics or inhibitor in ATDC5 cells. All slides were counterstained with DAPI (**E**). Bar charts showing the ratio comparisons of Ki67$^+$ cell numbers among different groups (**E1**). Scale bar 100 μm in (**E**). For each group in graphics, n = 3. Each bar represents mean ± S.D.; ANOVA: $^*P < 0.05$, $^{**}P < 0.01$, $^{***}P < 0.001$.

the chondrocyte differentiation in ATDC5 cells in presence of high glucose (Fig. 5). These data clearly confirmed that miR-322 was indeed involved in the pathological processes of chondrocyte proliferation and differentiation in growth plate in the context of congenital diabetes. However in the context of high-glucose environment, the expression of miR-322 increased during chondrocyte proliferation, but there were not significantly increases in the expression of Sox9 and pthlh (the proliferation markers) (Fig. 4C,D). This could be because high glucose itself inhibited cartilage proliferation, while miR-322 could not rescue this event unless it was overexpressed to a very high level. This might also be the reason for no changes in the ratio of PZ to total growth plate length in PGDM. And the possible reason for the relatively increased length of HZ in PGDM was that in a high-glucose environment, the expression of miR-322 decreased during chondrocyte differentiation, weakening its effect on differentiation inhibition.

Regarding what are the potential target genes for miR-322 to mediate chondrocyte proliferation and differentiation in the context of hyperglycemia, we employed down-expressed DEGs and four databases: miRDB, TargetScan, Starbase, and Tarbase to predict the potential miRNAs, and the corresponding result displayed that there were three potential target genes, i.e., Adamts5, Col12a1, and Cbx6, which were also verified by quantitative PCR (Fig. 6). The Adamts family is a group of proteases that act as key enzymes to catalyze the degradation of specific matrix components and regulate the renewal of the extracellular matrix. Among them, Adamts5 is involved in extracellular matrix degradation[45] and is related to arthritic cartilage breakdown[46]. In addition, Adamts5 may take part in the transdifferentiation of mast chondrocytes to osteoblasts[47], the differentiation of mesenchymal stem cells, as well as chondrocyte proliferation[48]. Col12a1 (type XII collagen) is a member of the protofibril-associated collagens[49] and is involved in bone formation by regulating osteoblast polarity and communication[50]. As a key gene in the early stages of cartilage tissue formation, Col12a1 is indispensable for cartilage differentiation and matrix accumulation[51]. Gene array analysis showed that the expression of Col12a1 increased, while Sox9 expression decreased at E15.0 compared to E13.0, and the expression of Col12a1 and Sox9 remained inversely proportional between E14.0 and E13.0[52]. This may partially explain our experimental results (Fig. 7A–E), as reduced expression of Col12a1 could lead to increased expression of Sox9, thus taking part in chondrocyte proliferation. Cbx6 (Chromobox6) is a subunit of polycomb repressive complex 1 (RC1) that plays a role in activity-mediated epigenetic regulation of gene expression. The function of the CBX6 gene has

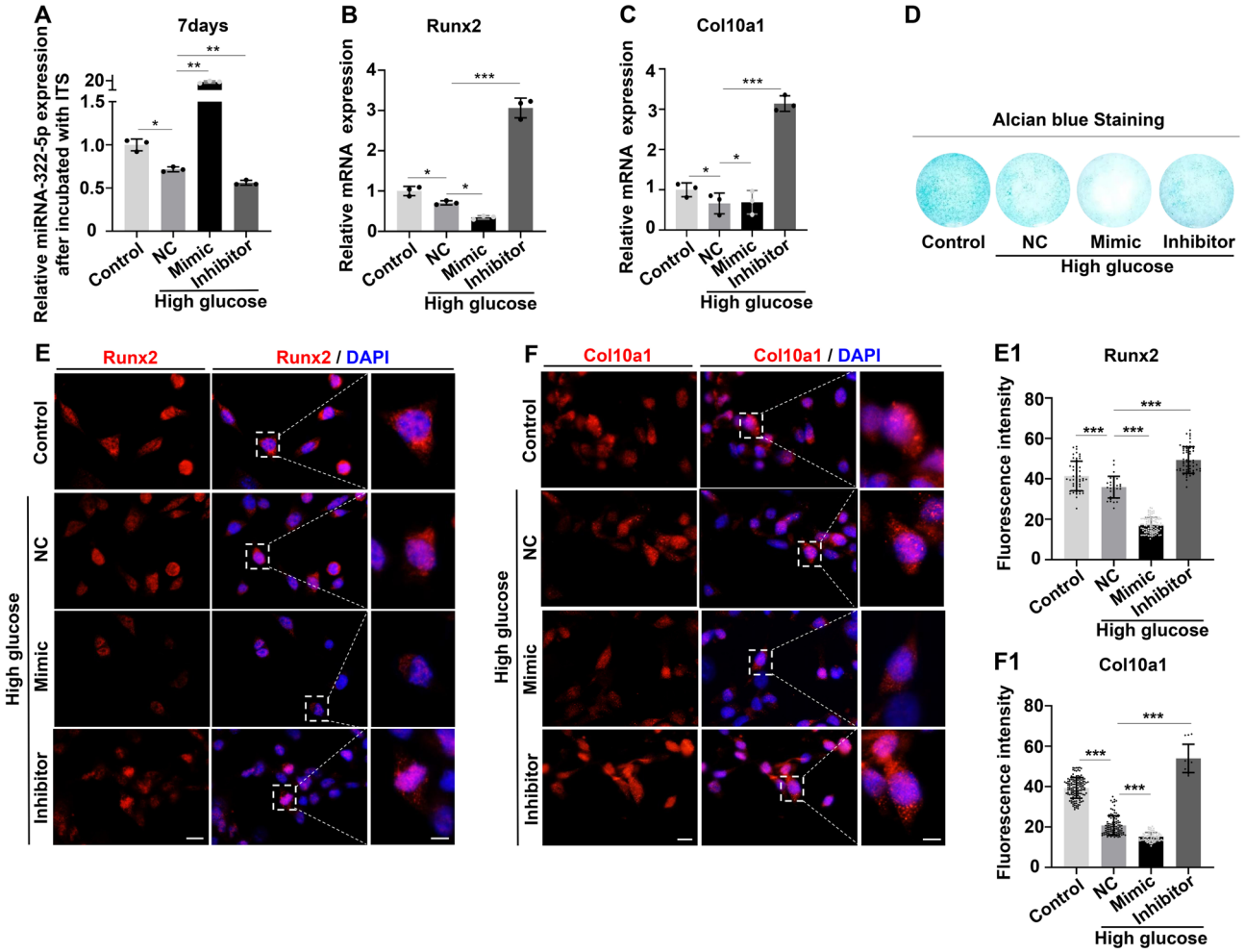

Figure 5. Determining the differentiation of chondrocytes in ATDC5 cells in presence of high glucose environment after manipulating miR-322 level. (**A**) The q-PCR data showing the expression level of miR-322 in ATDC5 cells in different groups after 7 days incubation following transfection. (**B**,**C**) The q-PCR data showing the expression of Runx2 (**B**) and Col10a1 (**C**) in ATDC5 cells, which were incubated for 7 days after transfected with miR-322 mimics or inhibitor. (**D**) Representative alician blue staining of ATDC5 cells incubated for 7 days after transfection with miR-322 mimics or inhibitor. (**E**,**F**) Representative immunofluorescence images of Runx2 (**E**) and Col10a1 (**F**) in ATDC5 cells transfected with miR-322 mimics or inhibitor. All slides were counterstained with DAPI. (**E1**,**F1**) Bar charts showing the comparisons of relative fluorescence intensities of Runx2 (**E1**) and Col10a1 (**F1**) in different groups. Scale bar 50 μm in the left and middle panels of (**E**) and (**F**), and 20 μm in the right panels. For (**E1**) and (**F1**), n = 200. For each group in graphics, n = 3. Each bar represents mean ± S.D.; ANOVA: $^{*}P < 0.05$, $^{**}P < 0.01$, $^{***}P < 0.001$.

currently limited to tumorgenesis, where it acted as an oncogene or tumor suppressor depending on the cancer type, but its role in cartilage has not yet been reported. Our experimental results (Fig. 7F–J) demonstrated that down-regulation of Cbx6 promoted chondrocyte proliferation. Additionally, existing research has indicated a relationship between Cbx6 and Snail/Zeb1[53], suggesting the neccessity for further investigating the role of Cbx6 in high-glucose-mediated chondrocyte proliferation. Thus, we manipulated the expression levels of Adamts5, Col12a1, and Cbx6 through transfection of their corresponding mimic and inhibitor in ATDC5 cells and then determined chondrocyte proliferation or differentiation and the relevant crucial gene expressions (Figs. 7, 8). The result demonstrated that Col12a1 and Cbx6 might act as the target genes on miR-322-regulated chondrocyte proliferation since their inhibitor transfection could successfully re-drop the increase of chondrocyte proliferation and relevant gene expressions (Sox9 and PthIh) induced by their mimic transfection (Fig. 7). Meanwhile, Adamts5, Col12a1 and Cbx6 probably work as the target genes on miR-322-regulated chondrocyte differentiation since their inhibitor transfection could successfully re-upregulate the drop of chondrocyte differentiation and relevant gene expressions (Runs2 and Col10a1) induced by their mimic transfection (Fig. 8).

In sum, the hyperglycemic state during pregnancy could interfere with the normal expression of miR-322 in the growth plate, and miR-322, in turn can target Adamts5, Col12a1, and Cbx6 and regulate the expressions of chondrocyte proliferation and differentiation-related genes, which would be the leading causes of abnormal chondrocyte proliferation and differentiation in growth plate of bone development caused by PGDM. However,

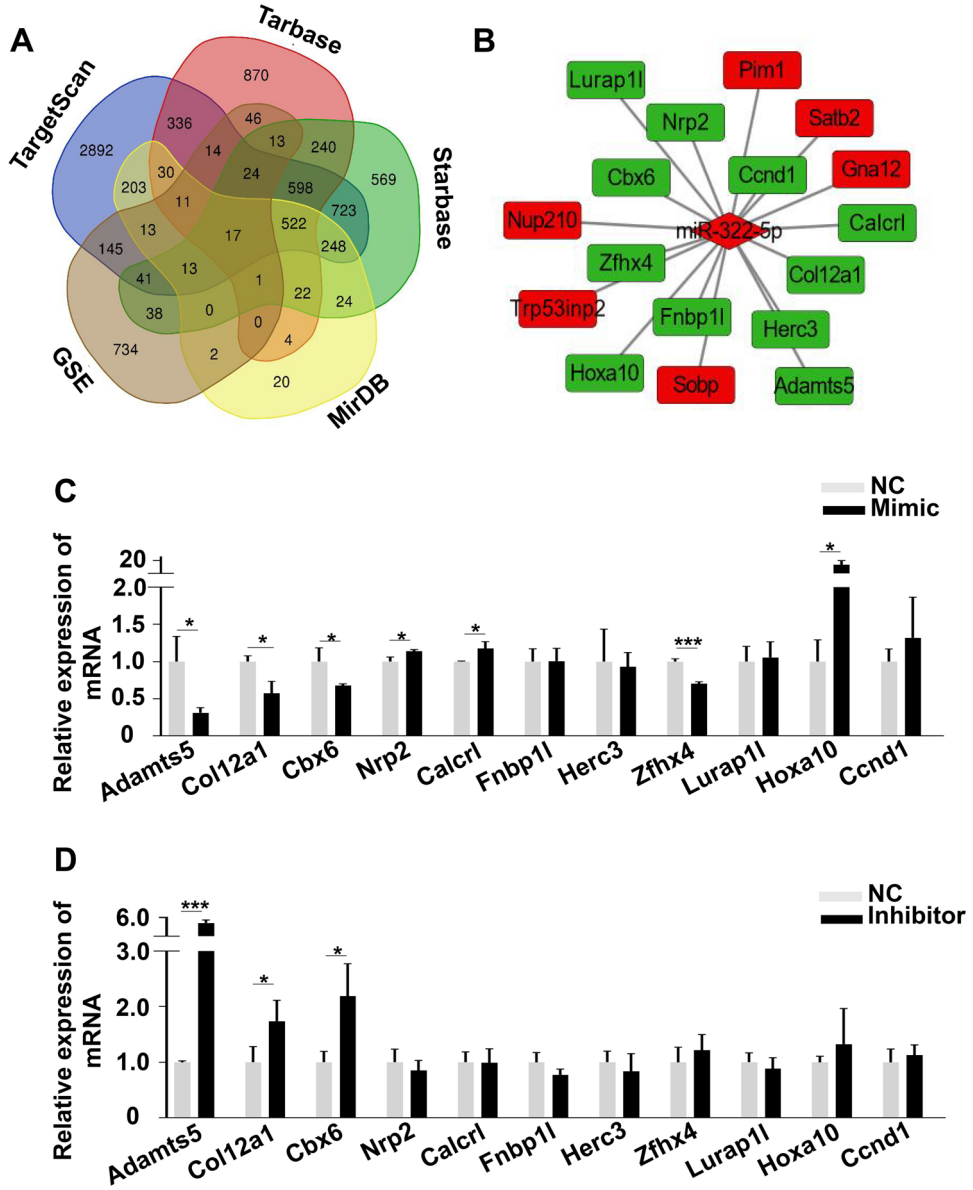

Figure 6. Prediction of miR-322 target genes and validation of putative target genes. (**A**,**B**) Venn diagram showing the down-regulated genes in DEG, which were taken to intersect with predicted genes of miR-322 to find potential target genes. (**C**,**D**) The q-PCR data showing the mRNA expressions of miR-322 potential target genes in ATDC5 cells transfected with miR-322 mimic (**C**) or inhibitor (**D**). For NC, mimic and inhibitor group, n = 3, respectively. Each bar represents mean ± S.D.; Student's t-test: $^{*}P < 0.05$, $^{**}P < 0.01$, $^{***}P < 0.001$.

some in vivo research, such as investigating the skeletal development of offspring from miR-322 knockout mice combined with diabetes during pregnancy, and dual-luciferase assay should be conducted for further study. There is no doubt that more precise biological studies on the underlying mechanism are required to develop a theoretical framework for clinical application (i.e., combat diabetic complications on fetal skeletal development) in the future.

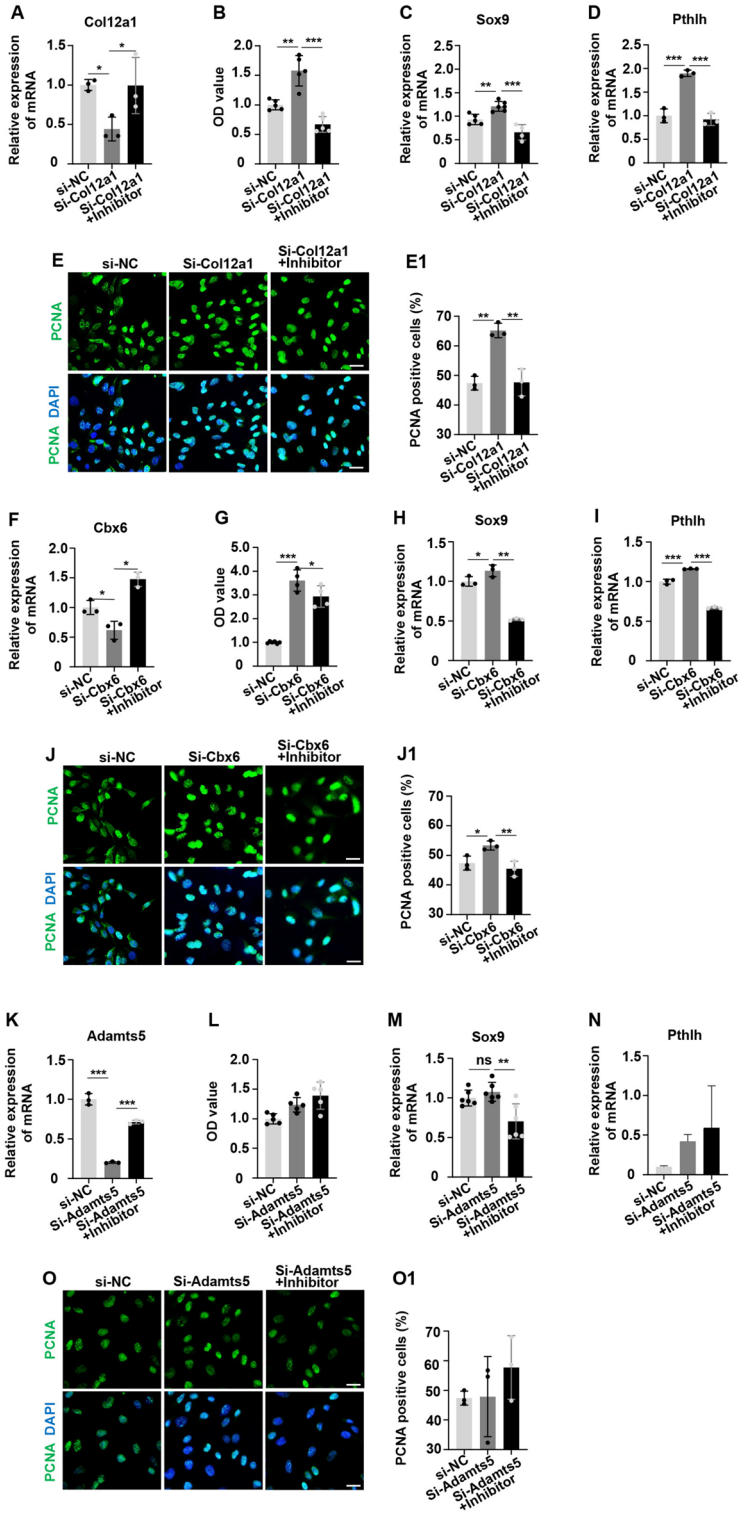

Figure 7. Determining the proliferation of chondrocytes using ATDC5 cells after manipulating miR-322 and its potential target gene levels. (**A**,**F**,**K**) The q-PCR data showing Col12a1 (**A**), Cbx6 (**G**), and Adamts5 (**M**) expression in ATDC5 cells transfected with si-NC, si-Col12a1, si-Cbx6, or si-Adamts5 and miR-322 inhibitor. (**B**,**G**,**L**) The cell viability was detected using CCK8 assay in the above cells. (**C**,**D**,**H**–**I**,**M**,**N**) The q-PCR data showing Sox9 (**C**,**H**,**M**) or Pthlh (**D**,**I**,**N**) expression in ATDC5 cells transfected with si-NC, si-Col12a1, si-Cbx6, si-Adamts5, or the co-transfected group with miR-322 inhibitor. (**E**,**J**,**O**) Representative images of PCNA immunofluorescent staining from the groups of si-NC, si-Col12a1, si-Cbx6, si-Adamts5, or the co-transfected group with miR-322 inhibitor. (**E1**,**J1**,**O1**) Bar charts showing the ratio comparisons of PCNA$^+$ cell numbers in different groups. Scale bar 100 μm in (**E**,**J**,**O**), and for each group in graphics, n = 3–5. Each bar represents mean ± S.D.; ANOVA: $^*P < 0.05$, $^{**}P < 0.01$, $^{***}P < 0.001$.

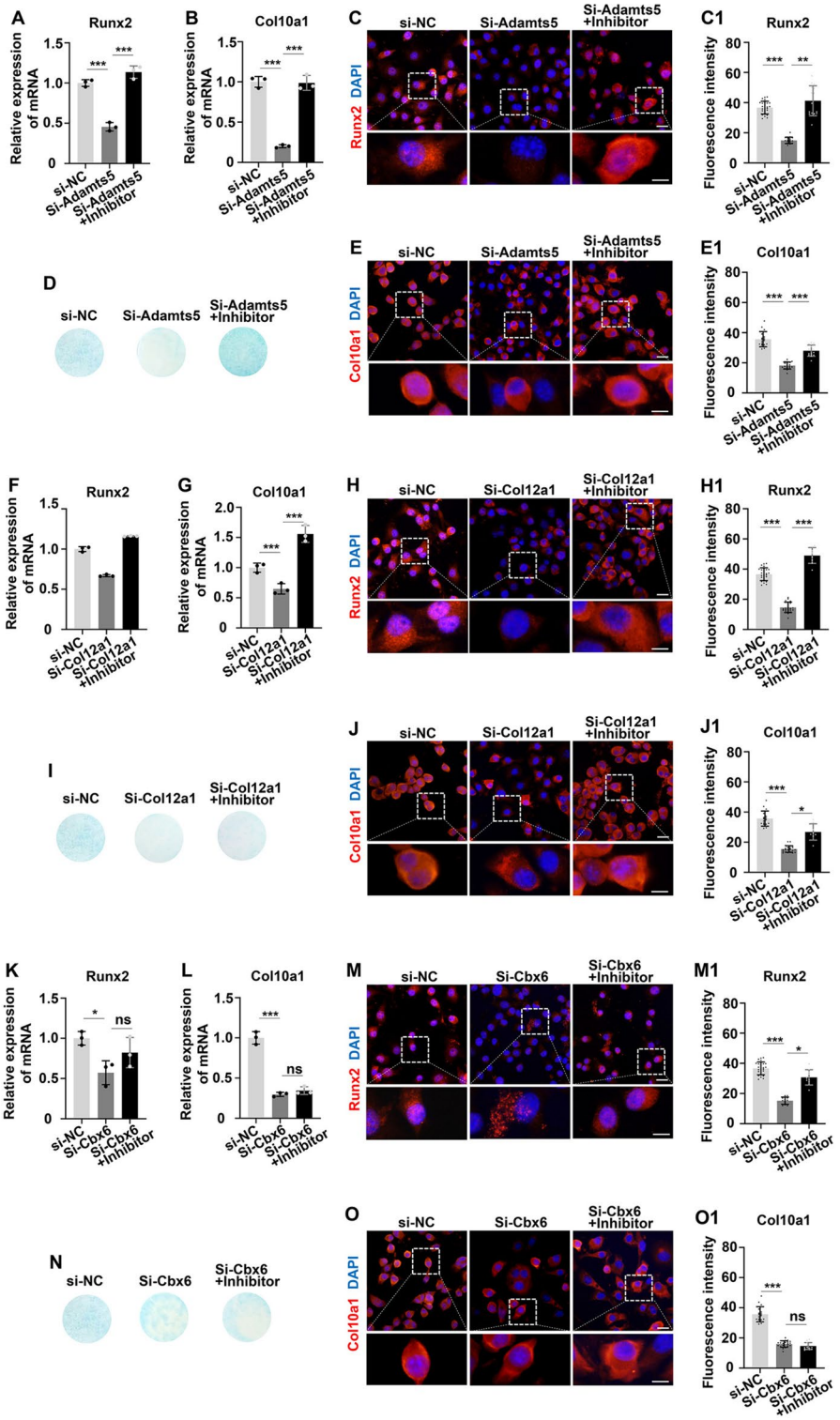

Figure 8. Determining the differentiation of chondrocytes using ATDC5 cells after manipulating miR-322 and its potential target gene levels. (**A**,**B**,**F**–**G**,**K**–**L**) The q-PCR data showing the expressions of Runx2 (**A**,**F**,**K**), and Col12a1 (**B**,**G**,**L**) in ATDC5 cells 7 days later following the above transfection. (**C**,**E**,**H**,**J**,**M**,**O**) Representative images of Runx2 (**C**,**H**,**M**) and Col10 (**E**,**J**,**O**) immunofluorescence in ATDC5 cells from si-NC, si-Adamts5, si-Col12a1, si-Cbx6 and the co-transfected group with miR-322 inhibitor. (**C1**,**E1**,**H1**,**J1**,**M1**,**O1**) Bar charts showing the comparisons of relative fluorescence intensities of Runx2 (**C1**,**H1**,**M1**) and Col10 (**E1**,**J1**,**O1**) among the above groups. (**D**,**I**,**N**) Alician blue staining in ATDC5 cells 7 days later following the above transfection. Scale bar 40 μm in the upper panel lines of (**C**,**E**,**H**,**J**,**M**,**O**); 20 μm in the lower panel of (**C**,**E**,**H**,**J**,**M**,**O**). For each group in (**A**,**B**,**F**–**G**,**K**–**L**), n = 3. For each group in (**C1**,**E1**,**H1**,**J1**,**M1**,**O1**), n = 200. Each bar represents mean ± S.D.; ANOVA: $^{*}P < 0.05$, $^{**}P < 0.01$, $^{***}P < 0.001$.

Data availability

The data that support the findings of this study are available in GEO at https://www.ncbi.nlm.nih.gov/geo. These data were derived from the following resources available in the public domain: GSE98036 , https://www.ncbi.nlm.nih.gov/geo/query/acc.cgi?acc=GSE98036; GSE7685, https://www.ncbi.nlm.nih.gov/geo/query/acc.cgi?acc=GSE7685.

Received: 27 April 2024; Accepted: 6 August 2024
Published online: 29 August 2024

References

1. Bánhidy, F., Acs, N., Puhó, E. H. & Czeizel, A. E. Congenital abnormalities in the offspring of pregnant women with type 1, type 2 and gestational diabetes mellitus: A population-based case-control study. *Congenit. Anom.* **50**, 115–121 (2010).
2. Whitehead, M. *et al.* Interrelations of calcium-regulating hormones during normal pregnancy. *Br. Med. J. (Clin. Res. Ed.)* **283**, 10–12 (1981).
3. Schushan-Eisen, I., Cohen, M., Leibovitch, L., Maayan-Metzger, A. & Strauss, T. Bone density among infants of gestational diabetic mothers and macrosomic neonates. *Matern. Child Health J.* **19**, 578–582 (2015).
4. Mimouni, F., Steichen, J. J., Tsang, R. C., Hertzberg, V. & Miodovnik, M. Decreased bone mineral content in infants of diabetic mothers. *Am. J. Perinatol.* **5**, 339–343 (1988).
5. Braddock, R., Simán, C. M., Hamilton, K., Garland, H. O. & Sibley, C. P. Gamma-linoleic acid and ascorbate improves skeletal ossification in offspring of diabetic rats. *Pediatr. Res.* **51**, 647–652 (2002).
6. Eriksson, U. J., Dahlström, E. & Hellerström, C. Diabetes in pregnancy. Skeletal malformations in the offspring of diabetic rats after intermittent withdrawal of insulin in early gestation. *Diabetes* **32**, 1141–1145 (1983).
7. Eriksson, U. J. Diabetes in pregnancy: retarded fetal growth, congenital malformations and feto-maternal concentrations of zinc, copper and manganese in the rat. *J. Nutr.* **114**, 477–484 (1984).
8. Aberg, A., Westbom, L. & Källén, B. Congenital malformations among infants whose mothers had gestational diabetes or preexisting diabetes. *Early Human Dev.* **61**, 85–95 (2001).
9. García-Patterson, A. *et al.* In human gestational diabetes mellitus congenital malformations are related to pre-pregnancy body mass index and to severity of diabetes. *Diabetologia* **47**, 509–514 (2004).
10. Simpson, J. L. *et al.* Diabetes in pregnancy, Northwestern University series (1977–1981). I. Prospective study of anomalies in offspring of mothers with diabetes mellitus. *Am. J. Obstetrics Gynecol.* **146**, 263–270 (1983).
11. Tinker, S. C. *et al.* Specific birth defects in pregnancies of women with diabetes: National Birth Defects Prevention Study, 1997–2011. *Am. J. Obstet. Gynecol.* **222**(176), e171-176.e111 (2020).
12. Adam, M. P. *et al.* Preaxial hallucal polydactyly as a marker for diabetic embryopathy. *Birth Defects Res. Part A Clin. Mol. Teratol.* **85**, 13–19 (2009).
13. Namgung, R. & Tsang, R. C. Bone in the pregnant mother and newborn at birth. *Int. J. Clin. Chem.* **333**, 1–11 (2003).
14. Kronenberg, H. M. Developmental regulation of the growth plate. *Nature* **423**, 332–336 (2003).
15. Jing, Y., Wang, Z., Li, H., Ma, C. & Feng, J. Chondrogenesis defines future skeletal patterns via cell transdifferentiation from chondrocytes to bone cells. *Curr. Osteopor. Rep.* **18**, 199–209 (2020).
16. Swingler, T. E. *et al.* The function of microRNAs in cartilage and osteoarthritis. *Clin. Exp. Rheumatol.* **37**(Suppl 120), 40–47 (2019).
17. Razmara, E. *et al.* Non-coding RNAs in cartilage development: An updated review. *Int. J. Mol. Sci.* **20**, 1 (2019).
18. Etich, J., Holzer, T., Pitzler, L., Bluhm, B. & Brachvogel, B. MiR-26a modulates extracellular matrix homeostasis in cartilage. *Matrix Biol. J. Int. Soc. Matrix Biol.* **43**, 27–34 (2015).
19. Jee, Y. H. *et al.* mir-374-5p, mir-379-5p, and mir-503-5p regulate proliferation and hypertrophic differentiation of growth plate chondrocytes in male rats. *Endocrinology* **159**, 1469–1478 (2018).
20. Papaioannou, G. *et al.* MicroRNA-140 provides robustness to the regulation of hypertrophic chondrocyte differentiation by the PTHrP-HDAC4 pathway. *J. Bone Mineral Res.* **30**, 1044–1052 (2015).
21. Grigelioniene, G. *et al.* Gain-of-function mutation of microRNA-140 in human skeletal dysplasia. *Nat. Med.* **25**, 583–590 (2019).
22. Edgar, R., Domrachev, M. & Lash, A. E. Gene Expression Omnibus: NCBI gene expression and hybridization array data repository. *Nucleic Acids Res.* **30**, 207–210 (2002).
23. Pomaznoy, M., Ha, B. & Peters, B. GOnet: A tool for interactive gene ontology analysis. *BMC Bioinformatics* **19**, 470 (2018).
24. Kanehisa, M., Furumichi, M., Tanabe, M., Sato, Y. & Morishima, K. KEGG: New perspectives on genomes, pathways, diseases and drugs. *Nucleic Acids Res.* **45**, D353–D361 (2017).
25. Ovchinnikov, D. Alcian blue/alizarin red staining of cartilage and bone in mouse. *Cold Spring Harbor Protocols* **2009**, pdb. prot5170 (2009).
26. Yang, G.-R., Dye, T. D. & Li, D. Effects of pre-gestational diabetes mellitus and gestational diabetes mellitus on macrosomia and birth defects in Upstate New York. *Diabetes Res. Clin. Pract.* **155**, 107811 (2019).
27. Cheng, X. *et al.* Microbiota-derived lipopolysaccharide retards chondrocyte hypertrophy in the growth plate through elevating Sox9 expression. *J. Cell. Physiol.* **234**, 2593–2605 (2018).
28. Wang, G. *et al.* Gut-lung dysbiosis accompanied by diabetes mellitus leads to pulmonary fibrotic change through the NF-κB signaling pathway. *Am. J. Pathol.* **191**, 838–856 (2021).
29. Janghorbani, M., Feskanich, D., Willett, W. C. & Hu, F. Prospective study of diabetes and risk of hip fracture: The Nurses' Health Study. *Diabetes Care* **29**, 1573–1578 (2006).
30. Räkel, A., Sheehy, O., Rahme, E. & LeLorier, J. Osteoporosis among patients with type 1 and type 2 diabetes. *Diabetes Metab.* **34**, 193–205 (2008).
31. Nieto, M. A., Patel, K. & Wilkinson, D. G. In situ hybridization analysis of chick embryos in whole mount and tissue sections. *Methods Cell Biol.* **51**, 219–235 (1996).
32. Acloque, H., Wilkinson, D. G. & Nieto, M. A. In situ hybridization analysis of chick embryos in whole-mount and tissue sections. *Methods Cell Biol.* **87**, 169–185 (2008).
33. Xu, S. *et al.* Dexamethasone interferes with osteoblasts formation during osteogenesis through altering IGF-1-mediated angiogenesis. *J. Cell. Physiol.* **234**, 15167–15181 (2019).
34. Liu, X. *et al.* NF-κB activation impedes the transdifferentiation of hypertrophic chondrocytes at the growth plate of mouse embryos in diabetic pregnancy. *J. Orthopaed. Transl.* **31**, 52–61 (2021).
35. Backes, C., Khaleeq, Q. T., Meese, E. & Keller, A. miEAA: microRNA enrichment analysis and annotation. *Nucleic Acids Res.* **44**, W110-116 (2016).
36. Cole, J. B. & Florez, J. C. Genetics of diabetes mellitus and diabetes complications. *Nat. Rev. Nephrol.* **16**, 377–390 (2020).
37. Bluhm, B. *et al.* miR-322 stabilizes MEK1 expression to inhibit RAF/MEK/ERK pathway activation in cartilage. *Development (Cambridge, England)* **144**, 3562–3577 (2017).

38. Gámez, B., Rodríguez-Carballo, E., Bartrons, R., Rosa, J. L. & Ventura, F. MicroRNA-322 (miR-322) and its target protein Tob2 modulate Osterix (Osx) mRNA stability. *J. Biol. Chem.* **288**, 14264–14275 (2013).
39. Gu, H. *et al.* The miR-322-TRAF3 circuit mediates the pro-apoptotic effect of high glucose on neural stem cells. *Toxicol. Sci. Off. J. Soc. Toxicol.* **144**, 186–196 (2015).
40. Zeng, Y. *et al.* Sox9-increased miR-322-5p facilitates BMP2-induced chondrogenic differentiation by targeting smad7 in mesenchymal stem cells. *Stem Cells Int.* **2021**, 9778207 (2021).
41. Georgieva, V. S. *et al.* Ablation of the miRNA cluster 24 in cartilage and osteoblasts impairs bone remodeling. *Sci. Rep.* **12**, 9116 (2022).
42. Georgieva, V. S. *et al.* Ablation of the miRNA cluster 24 has profound effects on extracellular matrix protein abundance in cartilage. *Int. J. Mol. Sci.* **21**, 1 (2020).
43. Kung, L. H. W. *et al.* Cartilage MicroRNA dysregulation during the onset and progression of mouse osteoarthritis is independent of aggrecanolysis and overlaps with candidates from end-stage human disease. *Arthritis Rheumatol.* **70**, 383–395 (2018).
44. Nemoto, T. & Kakinuma, Y. Fetal malnutrition-induced catch up failure is caused by elevated levels of miR-322 in rats. *Sci. Rep.* **10**, 1339 (2020).
45. Mokuda, S. *et al.* Wwp2 maintains cartilage homeostasis through regulation of Adamts5. *Nat. Commun.* **10**, 2429 (2019).
46. Glasson, S. S. *et al.* Deletion of active ADAMTS5 prevents cartilage degradation in a murine model of osteoarthritis. *Nature* **434**, 644–648 (2005).
47. Rogers-DeCotes, A. W., Porto, S. C., Dupuis, L. E. & Kern, C. B. ADAMTS5 is required for normal trabeculated bone development in the mandibular condyle. *Osteoarthritis Cartil.* **29**, 547–557 (2021).
48. Zhou, X. *et al.* MiR-132-3p regulates ADAMTS-5 expression and promotes chondrogenic differentiation of rat mesenchymal stem cells. *J. Cell. Biochem.* **119**, 2579–2587 (2018).
49. Gregory, K. E., Keene, D. R., Tufa, S. F., Lunstrum, G. P. & Morris, N. P. Developmental distribution of collagen type XII in cartilage: Association with articular cartilage and the growth plate. *J. Bone Mineral Res. Off. J. Am. Soc. Bone Miner. Res.* **16**, 2005–2016 (2001).
50. Izu, Y. *et al.* Type XII collagen regulates osteoblast polarity and communication during bone formation. *J. Cell Biol.* **193**, 1115–1130 (2011).
51. Taylor, D. W. *et al.* Collagen type XII and versican are present in the early stages of cartilage tissue formation by both redifferentating passaged and primary chondrocytes. *Tissue Eng. Part A* **21**, 683–693 (2015).
52. Veselá, B., Švandová, E., Bobek, J., Lesot, H. & Matalová, E. Osteogenic and angiogenic profiles of mandibular bone-forming cells. *Front. Physiol.* **10**, 1 (2019).
53. Deng, H. *et al.* CBX6 is negatively regulated by EZH2 and plays a potential tumor suppressor role in breast cancer. *Sci. Rep.* **9**, 197 (2019).

Acknowledgements

This study was supported by Natural Science Foundation of Guangdong Province (2021A1515012393), NSFC grant (82371692, 32170825), and Key laboratory of functional and clinical translational medicine, Fujian province university (XMMC-FCTM202101). We would like to thank Medical Experimental Center at Jinan University.

Author contributions

Fan Qian conceived and planned the experiments. Fan Qian and Xianlong Chen carried out the experiments. Fan Qian and Guang Wang planned and carried out the simulations. Simiao Wang, Min Liu and Yeyin Zhong were responsible for carrying out the experiments mentioned by reviewers. Xuesong Yang and Xin Cheng took the lead in writing the manuscript. All authors provided critical feedback and helped shape the research, analysis and manuscript.

Competing interests

The authors declare no competing interests.

Additional information

Supplementary Information The online version contains supplementary material available at https://doi.org/10.1038/s41598-024-69523-z.

Correspondence and requests for materials should be addressed to X.Y. or X.C.